IEEE Access
Multidisciplinary | Rapid Review | Open Access Journal

Received July 29, 2020, accepted August 27, 2020, date of publication August 31, 2020, date of current version September 14, 2020.

Digital Object Identifier 10.1109/ACCESS.2020.3020647

Next Generation Autofocus and Optical Image Stabilization System for Camera Modules Using Magnetic Shape Memory Actuators

NIKITA GABDULLIN, (Member, IEEE), HAMZA AHMAD, (Graduate Student Member, IEEE), AND JONGSUK RO, (Member, IEEE)

School of Electronic and Electrical Engineering, Chung-Ang University, Seoul 06974, South Korea

Corresponding author: Jongsuk Ro (jongsukro@gmail.com)

This work was supported in part by the Basic Science Research Program through the National Research Foundation of Korea funded by the Ministry of Education under Grant 2016R1D1A1B01008058, and in part by the Human Resources Development of the Korea Institute of Energy Technology Evaluation and Planning (KETEP) funded by the Korea Government Ministry of Trade, Industry and Energy under Grant 20204030200090.

ABSTRACT Currently, camera modules are used in a wide range of applications ranging from micropositioning actuator systems used in smartphones to larger modules used in stationary cameras, CCTV, and others. Modern camera modules are required to perform positioning functions to improve the stability and quality of captured images. These functions mainly include the autofocus (AF) and optical image stabilization (OIS) functions. Traditionally, separate actuators and sensors are used for AF and OIS, each contributing towards energy consumption, module size, and manufacturing costs. This is particularly disadvantageous in the case of smartphones owing to their inherent space and battery charge limitations. This paper presents a novel Magnetic Shape Memory (MSM) actuator system that combines the AF and OIS functions, which are performed using two actuators; thus, this system is a simple, compact, and cost-effective solution to the drawbacks of conventional technology. Furthermore, the smart properties of MSM alloys reduce the energy consumption of these systems through the utilization of their inherent holding forces and the associated shape memory effect. The realization of AF and OIS functions is discussed and verified experimentally for the proposed actuator system using data obtained from a fabricated prototype.

INDEX TERMS Autofocus, magnetic shape memory actuators, optical image stabilization, smart materials, smartphone camera module.

I. INTRODUCTION

Cameras have become indispensable in modern technology, as stand-alone applications, components of various devices such as smartphones, or a part of large-scale systems such as vehicles or closed-circuit television (CCTV) [1]. The properties of camera lenses determine the quality of captured images as well as the general capabilities of a camera. Moreover, the actuator elements that assist lens positioning and provide stabilization functions play a significant role in ensuring the high performance of camera modules. It is essential that mobile cameras used in biomedical applications are compact in size as well as highly accurate [2].

The associate editor coordinating the review of this manuscript and approving it for publication was Engang Tian.

Providing the aforementioned functions is particularly important in case of smartphones, wherein the performance of a camera significantly affects customer satisfaction and the functionality, price, and battery discharge rate of a smartphone. Furthermore, the height of the camera module is a limiting factor in the design of ultra-thin smartphones [3].

The primary positioning functions that a camera module actuator system must perform include the autofocus (AF) and optical image stabilization (OIS) functions. These functions require multiple specialized actuators in conventional camera modules [4]. However, this necessity of using several actuators increases the size of the camera module, complicates its control, increases its energy consumption, and decreases its reliability.

Conventionally, voice coil motor (VCM) actuator camera modules are used owing to their stable linear response and

low energy consumption in the case of light lenses. However, VCMs incorporate permanent magnets (PMs), which generate stray fields that could possibly affect the quality of captured images. Furthermore, each function and each degree-of-freedom in the system require a separate actuator, which in turn significantly complicates the structure of a complete AF/OIS camera module [4]. Furthermore, VCM technology also scales poorly because its size increases rapidly when large forces are required, which makes it unviable for heavy lens applications [5].

This paper presents an innovative camera module with a smart Magnetic Shape Memory (MSM) actuator system that can perform both AF and OIS functions. The proposed system only comprises two MSM actuators, both of which are involved in the realization of the AF and OIS functions. The smart properties of the MSM elements also facilitate a reduction in energy consumption through the utilization of inherent MSM holding forces. Furthermore, MSM actuators provide exceptional scalability, making the proposed technology viable for light micro-camera modules used in smartphones as well as for heavier lenses used in mobile and stationary cameras such as CCTVs.

II. MSM ALLOYS FOR CAMERA MODULE APPLICATIONS

A. MAGNETO-MECHANICAL RESPONSE OF MSM ALLOYS

MSM alloys, sometimes referred to as Ferromagnetic Shape Memory Alloys (FSMA), are relatively new smart materials that alter their shape in response to magnetic fields or mechanical stresses [6]. The most studied MSM alloys are Ni–Mn–Ga single-crystal alloys, which provide a shape change of 6–12% depending on their microstructure and also produce output stresses of up to 3 MPa [7]. The available strain in MSM alloys is greater than that in magnetostrictive or piezoelectric materials and reaches the level of thermally controlled shape memory alloys (SMAs).

SMAs are currently gaining popularity in camera [8] and wearable smart robotics [9] applications owing to their large strain and stress output [10]. However, their response time can be several seconds long during heating and even longer (10–30 s) during cooling [9], due to the high inertia of thermal expansion and contraction. Therefore, the application of SMAs in fast-response actuators is nearly impossible.

MSM alloys do not exhibit this disadvantage and respond fast to magnetic fields, with a reaction time of several milliseconds [11]; thus, they are potential candidates for application in electromagnetic actuators, sensors, and energy harvesters [12]. Furthermore, the smart properties of MSM alloys enable the design of self-sensing actuators which can be controlled by monitoring the state of the MSM element without the use of additional sensors [13], [14]. This simplifies the actuator system, as compared to traditional camera actuator technology [15].

Magnetic and mechanical responses are coupled in MSM alloys, and a combination of magnetic elongation with mechanical contraction is most widely used for actuator applications [16]. As shown in Fig. 1 (a), the elongation of an MSM element is proportional to the strength of a transversely applied magnetic field. This is due to the mutual interaction of the internal areas called variants, which are shown in green and blue in Fig. 1. Furthermore, due to the shape memory effect, the shape of the MSM alloy is maintained after the removal of the magnetic field [17]. A mechanical force should be applied to the MSM element to cause it to contract and to restore its shape, as shown in Fig. 1 (b). This mechanical force can be provided using a mechanical spring or another MSM element.

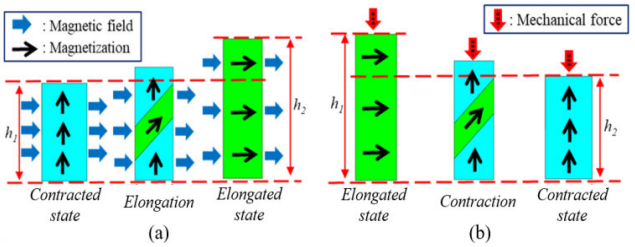

FIGURE 1. (a) Magnetic elongation and (b) mechanical contraction of MSM elements in actuators.

MSM alloys can also be used as SMAs when heated above their transformation temperature [18]. However, this method results in the loss of the advantages of magnetic actuation; therefore, this method is not considered in this study.

B. MAIN MSM ALLOY PARAMETERS FOR ACTUATOR APPLICATIONS

1) MAXIMUM STRAIN ε_{MAX} DETERMINED BY THE CRYSTALLOGRAPHIC DISTORTION IN SINGLE-CRYSTAL MSM ELEMENTS

This material parameter mainly depends on the composition and microstructure of the alloy. Typically, ε_{max} does not exceed 12% in the case of experimental alloys and averages 6% for a majority of commonly studied MSM alloy compositions [19], [20]. For practical engineering purposes, ε_{max} determines the maximum deformation of the MSM element; a further increase in magnetic or mechanical stresses does not result in a shape change. This has a direct impact on the size of MSM actuators and the entire actuator system.

2) TWINNING STRESS σ_{TW}

This parameter determines the holding force or maximum external force that the MSM element can sustain without undergoing a change in its shape. Therefore, this parameter is responsible for the shape memory effect. The twinning stress has the physical meaning of internal friction, and it contributes to the energy dissipation during actuation [21]. A low or a high twinning stress can be desirable depending on whether or not the holding force is exploited. However, it should be mentioned that this parameter is always nonzero in MSM alloys, and it mainly depends on the alloy microstructure and temperature. A majority of the studied Type I Ni–Mn–Ga MSM elements typically exhibit a

twinning stress of 0.5 MPa [22]. However, there is ongoing research on Type II Ni–Mn–Ga alloys that have twinning stresses less than 0.1 MPa [23], [24]. As presented in this paper, the latter can reduce the "dead zone" at low currents in the MSM actuator system, which can be beneficial for the proposed camera module design.

3) MAGNETIC STRESS σ_{mag}

This parameter determines the maximum stress that the MSM element produces when subjected to magnetic fields. Hence, this parameter determines the maximum output force for an MSM element with a fixed size. The magnetic stress is primarily determined by the MSM alloy microstructure and is commonly considered to not exceed 3 MPa [25], [26]. However, alloys with magnetic stress as high as 3.5 MPa have also been reported [27].

The three parameters discussed above must be taken into consideration when selecting MSM alloys for camera module applications, because altering the alloy composition may result in an improvement in one of the parameters at the expense of another.

III. MSM ACTUATOR SYSTEM FOR A COMBINED AF/OIS CAMERA MODULE

A. STRUCTURE AND OPERATING PRINCIPLES OF THE PROPOSED MSM ACTUATOR FOR CAMERA MODULE APPLICATIONS

The proposed AF/OIS MSM actuator system shown in Fig. 2 allocates the lens barrel in a holder between two MSM elements connected to mechanical springs. The magnetic fields for elongation described in Fig. 1 (a) are produced by coils and guided by flux guide (not shown) and controlled by varying the amplitudes of the coil currents. The mechanical force for contraction, described in Fig. 1 (b), is produced using compressive springs that oppose the MSM forces in each actuator.

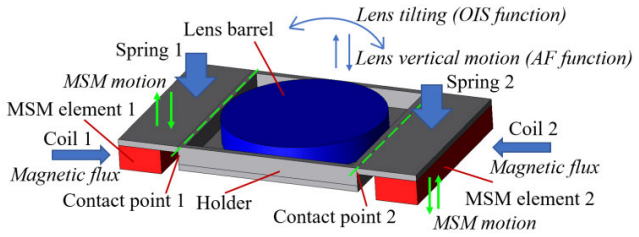

FIGURE 2. Combined AF/OIS MSM actuator system design for camera module applications.

Whereas it is possible to design MSM actuators with magnetically-initiated contraction, it requires spatially rotating the magnetic field by 90° unlike in other electromagnetic actuators where changing the polarity of supply voltage or current reverses the electromagnetic force. Thus, magnetic circuits of such actuators become sophisticated and have significantly higher reluctance due to the necessity to conduct the magnetic field along the length of low-permeability MSM element instead of high permeability core [16], [28]. Thus, the MSM actuator system with magnetic elongation and mechanical contraction presented in this paper is more suitable for practical applications.

B. PERFORMING THE AF FUNCTION

Each side of the holder is connected between the MSM element and a corresponding spring. The connection is such that the lens barrel can be moved or tilted by changing the spatial orientation of the holder. This allows the positions of the holder's contact points 1 and 2 to be controlled by adjusting the lengths of the MSM elements.

A camera module actuator must be capable of moving the lens barrel linearly to realize the AF function. In the proposed MSM actuator system, this is achieved by controlling the lengths of both MSM elements simultaneously. Energizing both coils results in the same strain in both MSM elements; thus, the lens barrel moves linearly upwards, as shown in Fig. 3. However, decreasing the currents in both coils results in a corresponding decrease in the magnetic stresses in the MSM elements, thereby enabling the springs to contract them. This results in the downward motion of the lens barrel.

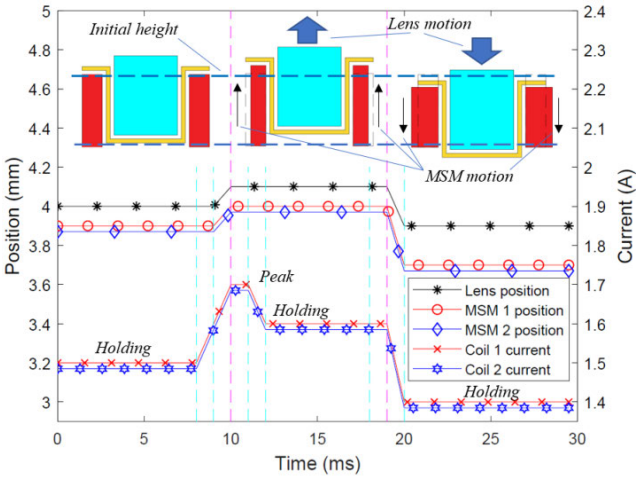

FIGURE 3. Operating principle of the proposed actuator system performing the AF function. Current and displacement numerical values are for reference only.

The total travel distance depends on the strain of the MSM elements and the weight of the lens. Typical MSM elements produce large strain outputs exceeding 1 mm when standard 15-mm samples are used [28], [29]. However, the AF displacement that is required in camera module applications is typically less than 0.2 mm; hence, it can be realized via MSM elements with a height of less than 4 mm due to their large available strain. Performing AF function with short MSM elements illustrates the potential for designing compact, miniaturized camera modules for thin smartphones.

C. PERFORMING THE OIS FUNCTION

There are multiple methods of realizing the OIS function in conventional camera modules, including multiple degree-of-freedom (DOF) motion in one plane and tilting the camera

module [30], [31]. Traditionally, at least two additional actuators are required to realize the OIS function in an actuator system that performs the AF function. Remarkably, the proposed MSM actuator system can tilt the lens barrel using the same MSM elements that perform the AF function. Therefore, additional actuators or active elements are not required.

Fig. 4 indicates that a decrease in the length of one MSM element while the state of the other element remains unchanged results in the lens barrel tilting towards the contracting MSM element. For example, due to the contraction of the MSM element 1 shown in Fig. 2, the contact point 1 moves downwards and the lens barrel holder pivots on the contact point 2 (see Fig. 4). Similarly, contracting the MSM element 2 results in the camera module pivoting on the contact point 1. The tilt angle is proportional to the difference in the lengths of MSM elements 1 and 2. Hence, OIS is realized by controlling the *length difference*, whereas the AF function is realized by controlling the *total lengths* of the MSM elements.

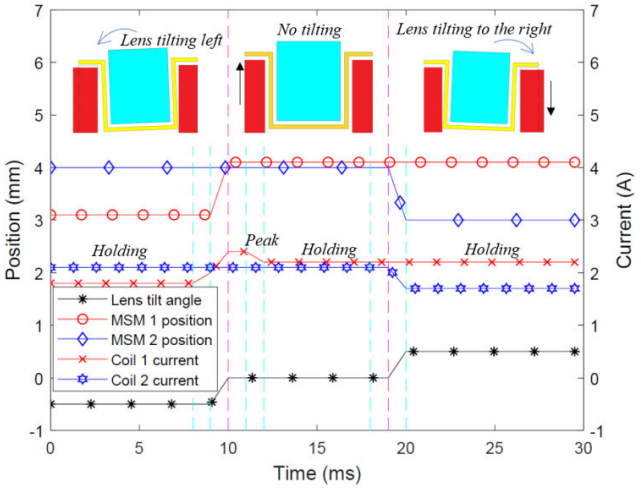

FIGURE 4. Operating principle of the proposed actuator system performing the OIS function. Current, displacement, and tilt angle numerical values are for reference only.

It should be noted that the OIS and AF functions can be controlled independently or can be combined by linearly moving a tilted camera module. Therefore, performing one function does not obstruct the other, and both functions can be performed simultaneously.

IV. ANALYSIS AND DESIGN OF MSM ACTUATORS

A. MAIN DESIGN PARAMETERS OF MSM ACTUATORS FOR CAMERA MODULE APPLICATIONS

The proposed MSM actuator system includes two identical actuators shown in Fig. 5. This structure is typical for MSM actuators and consists only of an MSM element, a flux guide, and a coil. This structure ensures the largest strain output for the lowest flux guide size [32]. Traditional considerations for the design of flux guides that are commonly used in electrical machines are applicable to the design of the MSM actuator flux guide [33]. However, when designing smartphone camera modules, the design of the core section that accommodates the coil is different, owing to the height constraints due to space limitations.

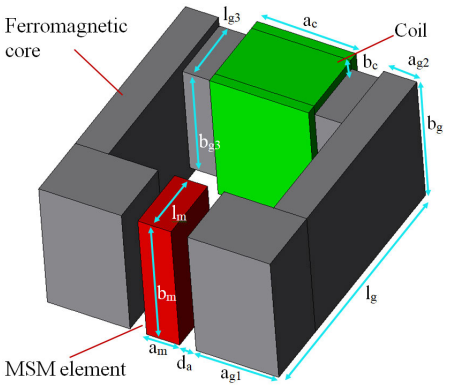

FIGURE 5. Magnetic circuit parameters of the proposed MSM actuator for camera module applications.

The main design parameters for the MSM actuator system are the maximum displacement d_{max}, maximum tilt angle θ_{max}, maximum lens mass m_l, and total height of the actuator system h_{tot}. Typically, in MSM actuators the parameters of the MSM element influence other parameters of the circuit [32]. Fig. 5 shows that the total height of the magnetic circuit is determined by the height of the MSM element b_m where

$$b_m = \frac{d_{max}}{\varepsilon_{max}} \tag{1}$$

Equation (1) shows that MSM alloys with larger values of ε_{max} facilitate the design of MSM actuators featuring smaller heights; hence, these alloys are more suitable for thin smartphones. It must be noted that, while magnetically controlled MSM alloys with $\varepsilon_{max} > 12\%$ have been discussed by other researchers, these alloys can currently only be controlled mechanically because their twinning stress exceeds their magnetic stress [34]. Therefore, only MSM alloys with $\varepsilon_{max} = 6\%$ are considered in this study.

The width of the MSM element a_m is the main contributor to the reluctance of the air gap and should be minimized. However, it is difficult to manufacture MSM elements with $a_m < 0.5$ mm. Similarly, although narrow air gaps are desirable, manufacturing air gaps with $d_m < 0.1$ mm is typically impossible. Finally, the length of the MSM element l_m is determined by considering the desired output force as

$$l_m = \frac{F_{max}}{\sigma_{mag} \cdot a_m} \tag{2}$$

where F_{max} is the maximum magnetic force among all the possible regimes. As discussed in Section IV-C, this force is mainly required to overcome the weight of the lens barrel, which implies that the maximum allowed lens weight is determined by the magnetic stress of the MSM element and its cross-sectional area. As an increase in a_m also results in an increase in the reluctance of the magnetic circuit, l_m is usually

increased to increase the output force without compromising other parameters of the MSM actuator.

In smartphone applications, to accommodate the coil without increasing the total height, the height of a core section near the coil should be reduced by the height of the coil window b_c

$$b_{g3} = b_m - 2b_c \tag{3}$$

To compensate for this reduction while preserving the same flux density throughout the magnetic circuit, the length of the core that accommodates the coil is increased so that

$$l_{g3} = \frac{b_m \cdot l_m}{b_{g3}} \tag{4}$$

Finally, the maximum tilt angle for OIS is calculated using simple trigonometry (derivation omitted), while considering the lens diameter d_l and lens holder width a_h as follows:

$$\theta_{max} = \text{asin}(\frac{d_{max}}{d_l + 2a_h}) \tag{5}$$

where d_l is the lens diameter, and a_h is the width of the lens holder wall.

B. ELECTROMAGNETIC ANALYSIS OF MSM ACTUATORS

Although the MSM behavior has been discussed in a simplistic manner in Section II, some of its aspects make an accurate MSM actuator analysis extremely complicated. Because ''easy'' variants grow during elongation and their permeability is greater than that of ''hard'' variants, an MSM element is non-homogeneous and anisotropic during its shape change, and its overall permeability changes in a nonlinear manner [35], [36]. Furthermore, it becomes thinner as it elongates, further affecting the parameters of the magnetic circuit.

Currently, finite element analysis (FEA) is the most commonly used analysis method for electromagnetic actuator designs; however, none of the commercially available software packages are capable of modeling all aspects of MSM behavior in a straightforward manner. Several recently proposed methods allow the MSM performance to be evaluated based on an electromagnetic analysis using traditional FEA software, such when the experimental strain–stress curves shown in Fig. 6 is used for force and strain calculation [11], [17]. This enables the estimation of the MSM actuator performance via an analysis of the magnetic field in the air gap as well as the estimation of the MSM element state using the data shown in Fig. 6 [11], [37].

Furthermore, for the purposes of estimating the design parameters and verifying the feasibility of the proposed MSM actuator system, the 2D FEA shown in Fig. 7 can be used to realize a faster analysis with sufficient accuracy. However, for the final design optimization, a complete 3D FEA is required [35]; this is beyond the scope of this study, which is focused on the verification of the operating principles.

The simplified lumped parameter model shown in Fig. 8 can further assist in understanding the behavior of MSM actuator parameters when the strain changes [35]. It is useful to represent the MSM element as a single element with

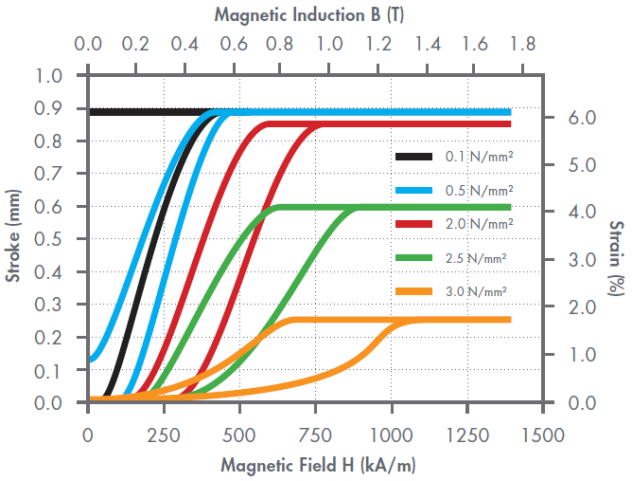

FIGURE 6. Experimental strain–stress curves for MSM alloys (courtesy of [11]).

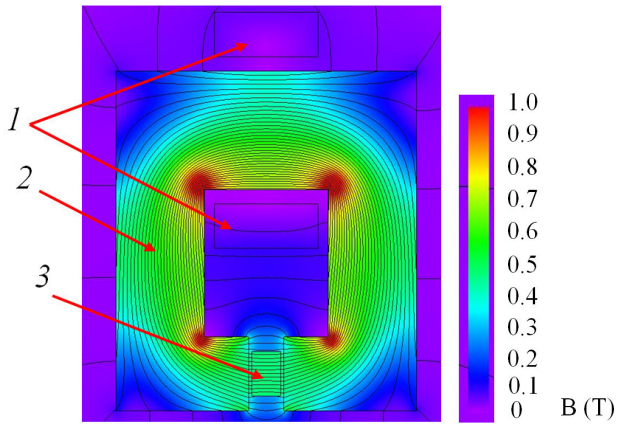

FIGURE 7. Magnetic field distribution in the magnetic circuit of MSM actuator (top view) guiding the magnetic flux produced by the coil (1) in actuator core (2) to the MSM element (3).

reluctance R_{msm} and effective relative permeability μ_m, as this facilitates the representation of the air gap region shown in Fig. 8 (a) using the simple circuit shown in Fig. 8 (b) when the saturation effects are neglected. This enables an investigation of the general trends of MSM actuator dynamics without having to deal with the complexities of the non-homogenous and anisotropic MSM behavior. Upon solving the simple magnetic circuit shown in Fig. 8 (b) for the coil current required to generate a magnetic field intensity H_a that corresponds to the desired strain (see Fig. 6), we obtain

$$I_c = \frac{H_a}{w_c} \cdot (2d_a + \frac{a_m}{\mu_m}) \tag{6}$$

where w_c is the number of coil turns. Equation (6) shows that the required current I_c is proportional to the air gap size and the MSM element width divided by the MSM effective relative permeability. Hence, a smaller air gap, thin MSM element, and higher MSM permeability are desirable for reducing power consumption. The overall behavior of the

MSM actuator output can be expected to be similar to that expressed by the curves in Fig. 6, owing to the interrelation among coil current, magnetic field, and MSM element shape.

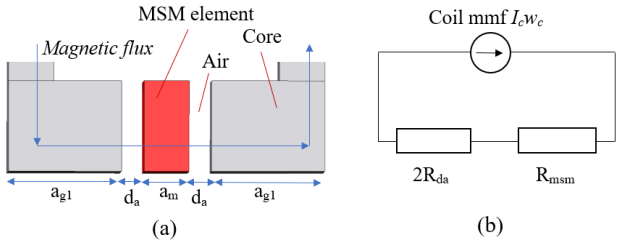

FIGURE 8. (a) Top view of the air gap region of the MSM actuator with (b) its simplistic lumped parameter representation assuming infinite core permeability.

C. FORCES ACTING ON MSM ELEMENTS IN CAMERA MODULES

An MSM camera module is essentially a positioning system; thus, magnetic forces F_{mag} generated by the MSM elements are only required to compensate the friction F_{fr} and gravitational forces. However, the compressive forces F_{comp} associated with the springs and the holding forces of MSM elements F_{hold} should also be taken into consideration. Upon applying Newton's laws of motion to the proposed actuator system, we obtain the following force balance equations for each MSM element:

$$\begin{cases} F_{mag}(I_c) = F_{comp}(x) + F_{hold} + F_{grav} + F_{fr} \\ F_{mag}(I_c) = \sigma_{mag}(I_c) \cdot a_m \cdot l_m \\ F_{hold} = \sigma_{tw} \cdot a_m \cdot l_m \\ F_{grav} = 0.5\,(m_l + m_h)\,g \\ F_{comp}(x) = k_{spring} \cdot (x_{in} + \Delta x) \end{cases} \tag{7}$$

where k_{spring} is the spring coefficient in N/m, x_{in} is the initial pre-strain of the spring in m, Δx is the lens displacement in m, m_l and m_h are the masses of the lens barrel and lens holder in kg, respectively, and g is the gravitational constant.

Equation (7) shows that, even in the absence of an external load and compressive springs, the magnetic forces are still opposed by the inherent MSM holding forces that are responsible for the initial offset of the curves in Fig. 6. However, external mechanical loads are also opposed by these holding forces, thereby resulting in a shape memory effect that allows the lens position to be maintained at a reduced or even zero coil current, as previously mentioned in Section III.

However, it should be noted that constant force springs are most suitable for MSM camera modules because MSM holding forces are almost independent of the lens position x as shown in (7). Thus, it is desirable that the change in $F_{comp}(x)$ with x is close to zero, which can be achieved with zero-free-length springs or springs wherein $x_{in} \gg \Delta x$ [38], [39].

D. MSM ACTUATOR DESIGN FLOW

Based on the discussion in this section, Fig. 9 presents the proposed design strategy for MSM actuators to be used in camera module applications. Considering the desired lens weight and AF/OIS motion range, (7) is used to estimate the forces that the MSM actuator system needs to develop, thereby facilitating the selection of the size of MSM elements. The complete magnetic circuit is then designed to accommodate the MSM element and ensure the production of a magnetic field that is sufficient for the desired output according to Fig. 6.

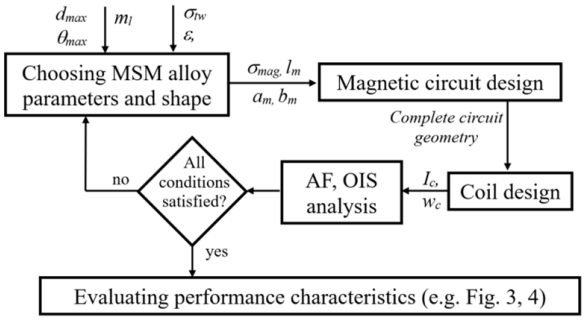

FIGURE 9. Proposed design flow for MSM camera module actuators.

V. EXPERIMENTAL VERIFICATION OF AF AND OIS FUNCTIONS

A. MSM ACTUATOR AND MSM ACTUATOR SYSTEM PROTOTYPES

In order to verify the proposed actuator system, which combines the AF and OIS functions, two identical actuators shown in Fig. 10 were fabricated. Two 2 × 3 × 15 mm Ni_2MnGa MSM elements used in the verification prototypes were provided by ETO Magnetic, Germany. Table 1 summarizes the design parameters of the prototype actuators. Housing box and mechanical springs were removed for the clarity of the verification experiment.

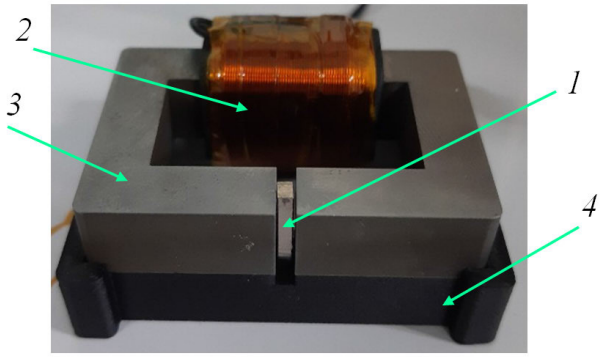

FIGURE 10. MSM actuator prototype including (1) MSM element, (2) coil, (3) core, and (4) housing.

It should be noted that the verification prototype was not subjected to any size restrictions for clarity of the experiment. Thus, height minimization was not required and the actuators were fabricated with core of uniform height. To accommodate

TABLE 1. Design parameters of MSM actuator for camera module.

Parameter	Value	Parameter	Value
Number of coil turns w_c	700	l_g	24 mm
a_c	12 mm	a_{g1}	10 mm
MSM alloy	Ni_2MnGa	d_a	0.2 mm
a_m	2 mm	l_{g3}	6 mm
b_m	15 mm	b_g	15 mm
l_m	3 mm	a_{g2}	4 mm

the coil and ensure the mechanical stability of the actuators, the core with a wound coil was positioned on a 3D-printed housing which was also used to stabilize the MSM element so that elongation occurs only at its free end.

Fig. 11 presents the experimental setup for the verification of the AF/OIS function. In addition to the MSM actuators, the Keyence LK-35 high-precision laser position sensor and N5751A DC current source by Agilent Technologies are also used. The AF and OIS functions are verified at no-load conditions and under a 65 g load (where a coin stack representing a lens barrel was attached to the connector).

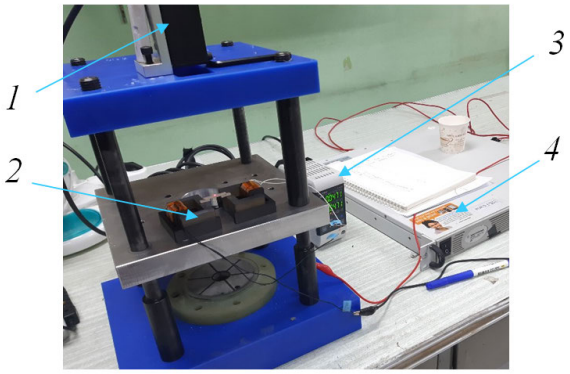

FIGURE 11. Experimental setup for AF/OIS function verification that includes (1) a laser head, (2) MSM actuator system, (3) a measurement unit, and (4) DC current source. The laser measures the position of a point on the connector placed between two MSM actuators.

B. EXPERIMENTAL VERIFICATION OF THE AF FUNCTION

Fig. 11 shows that the MSM elements in actuators are connected using a rod connector for the purposes of position measurement. As both MSM elements are required to be excited to realize the AF function, the position of the center of the rod is measured during this experiment. Here, both actuators are connected to power sources and are excited using DC currents of the same magnitude.

In the no-load condition, only the connector is present. However, additional experiments are conducted using a 65 g coin stack attached to the rod to imitate the weight of the lens barrel, in order to verify the AF function under a load, as shown in Fig. 12.

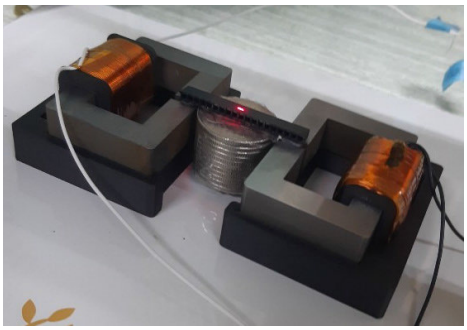

FIGURE 12. MSM actuator system loaded with a 65-g coin stack for imitating lens weight to verify AF function under load. The position is measured at the middle of the connector.

Fig. 13 shows that the connector position follows the displacement trends of the MSM alloys shown in Fig. 6. At the no-load condition, displacement is not observed up to 0.2 A, which can be attributed to the magnetic field required to overcome the twinning stress of the MSM elements. Upon reaching 0.2 A, a nearly linear response is observed up to 1.1 A, where the AF displacement reaches 1.1 mm, thereby indicating the maximum elongation of the MSM elements. A further increase in the current does not result in a position change. This behavior strongly resembles the 0.1 N/mm^2 curve shown in Fig. 6, which can be expected for an unloaded MSM actuator system.

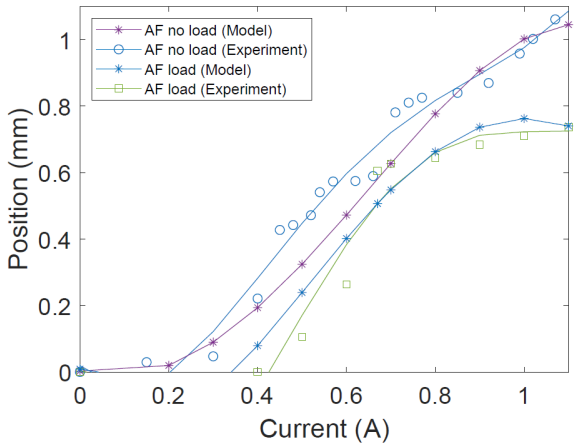

FIGURE 13. Comparison of analysis results and experimental data for AF function verification at 65 g and zero load.

When a 65 g load is added to the connector, the minimum required current increases because the weight of the loads increases the total force acting on the MSM elements in (7). Although the maximum AF displacement is reduced, it still reaches 0.7 mm, which is considerably large for AF actuators. A current range of 0.4 A to 0.9 A also ensured an almost linear response, which is desirable for AF applications. This behavior is similar to that of the 2.5 N/mm^2 curve shown in Fig. 6, thus indicating a good agreement between theory and experiment. The power consumption of the verification

prototype was about 10 W at maximum strain, and 3−5 W for intermediate strains. It should be noted that this prototype was designed to verify the possibility of combining the AF and OIS functions and was not optimized for power consumption, which could be reduced by minimizing the magnetic circuit reluctance to reduce the required current.

In both experiments, the holding of the final and all intermediate AF positions was observed owing to the shape memory effect. This demonstrates the energy saving potential of MSM technology when the holding forces are appropriately utilized. However, this design relies on the compressive springs for the shape restoration. Therefore, a non-zero holding current is required for maintaining the AF position, as previously shown in Fig. 3.

C. EXPERIMENTAL VERIFICATION OF THE OIS FUNCTION

The purpose of the OIS verification experiment is to measure the tilt angle of the camera module, which is realized by measuring the displacement of one side of the connector rod while maintaining the other side at a fixed position. Fig. 14 shows the position of the measurement point for a case where the right MSM actuator was being excited; hence, the rod tilts to the left. However, due to the symmetry of the system, the results discussed below are applicable to both right and left tilt directions.

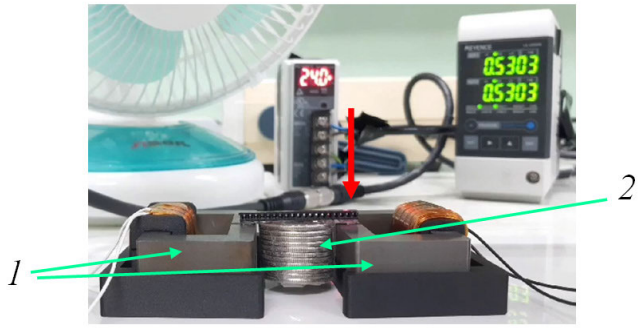

FIGURE 14. MSM actuators (1) loaded with a coin stack (2) imitating lens barrel for OIS function verification. A red arrow (in color) shows the position of the measurement point on the side of the connector adjacent to the excited MSM element.

Fig. 15 shows a behavior similar to that in Fig. 13, with the initial current offset affected by the MSM twinning stress and the applied load. For the no-load condition, a maximum tilt angle of 1.4° was observed. This angle is proportional to the MSM element elongation, as can be expected based on the discussion in Section III-C. This angle is reduced to 1° when the load is applied.

VI. DISCUSSIONS

A. COMBINING AF AND OIS FUNCTIONS IN MSM ACTUATOR SYSTEM

The discussion in Section II and the experimental results presented in Section V prove that the proposed MSM actuator system successfully combines both linear motion and lens

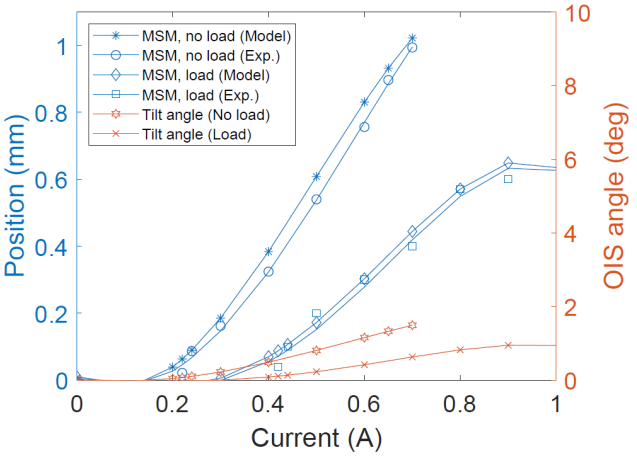

FIGURE 15. Comparison of analysis results and experimental data verifying OIS function at 65 g and zero load.

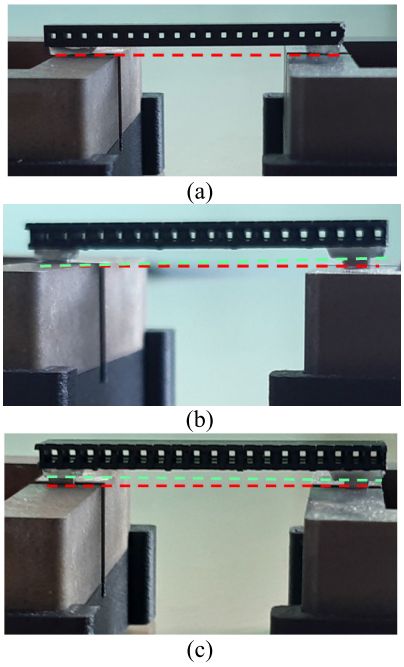

FIGURE 16. The proposed actuator system consequently performing AF and OIS functions. (a) The initial state (shown by the red dashed line) with both MSM elements contracted, (b) tilting the connector by elongating the right MSM element to perform the OIS function, and (c) elongating left MSM element to align the connector horizontally and thus perform the AF function.

barrel tilting, thereby realizing the AF and OIS functions using two actuators. As expected, elongating both MSM elements realizes the AF function, whereas controlling the length difference between the MSM elements allows the OIS function to be performed. Furthermore, the possibility of controlling both the tilt angle and the lens height indicates that AF and OIS functions can be performed consequently and controlled independently. This is shown in Fig. 16 where the OIS function is performed by elongating one of the MSM elements (see Fig. 16 (b)), and then another one is elongated

aligning the connector horizontally at a position different from the initial one (Fig. 16 (c)), thus performing the AF function.

Combining the AF and OIS functions in a camera module actuator system using only two actuators substantially reduces the complexity of the system and the number of components and active elements, potentially increases system reliability, and reduces energy consumption and discharge rate of batteries in mobile devices.

B. ADVANTAGES OF THE CAMERA MODULE MSM ACTUATOR SYSTEM

As previously mentioned, one of the main advantages of the proposed MSM actuator camera module is the reduction in the number of actuators required to realize the AF and OIS functions. Conventionally, the OIS function alone requires at least three actuators, and additional one or two actuators are required for the AF function. Therefore, the proposed design at the least halves the number of active elements in the actuator system, compared to conventional technology.

Although MSM alloys are magnetic, their magnetization is relatively low; thus, there is nearly no magnetic field generated by the alloy. Conversely, in VCM camera module actuators strong PMs are positioned close to or directly on the lens barrel, thus inevitably subjecting the lens to stray magnetic fields potentially affecting the captured image quality. Therefore, the adverse influence of the aforementioned magnetic fields is eliminated in the proposed design due to the absence of PMs. Furthermore, VCM coils are also positioned close to the lens barrel because the electromagnetic forces between the coils and PMs act in free air requiring close proximity for better performance. Thus, both PM and coil magnetic fields can be linked with the lens in VCM camera modules. On the contrary, in the proposed MSM actuator system the coils are removed from the lens barrel minimizing the effects of coil leakage flux on the lens, whereas high-permeability core guides the main magnetic flux to the MSM element. Hence, only a small portion of flux leakage in the MSM region can potentially reach the lens unlike in VCM-based camera modules.

Furthermore, the curves in Fig. 6 and the data shown in Fig. 13 and Fig. 15 indicate that the MSM actuator system can produce large forces even when the MSM elements are considerably elongated. While the maximum available strain decreases as the load increases, in the allowed operating range the force is essentially independent of the strain. This is desirable in positioning systems wherein a constant force, such as gravity, needs to be compensated. Hence, this is a considerable advantage that enables the use of heavier lenses, unlike conventional electromagnetic actuators where the force decreases as the square of the distance, which is only suitable for micropositioning systems.

The verification prototype presented in this paper was fabricated using MSM elements of standard size which can be changed depending on the application following the recommendations proposed in this paper. An extremely large displacement produced by the system shown in Fig. 13 and Fig. 15 greatly exceeds the commonly required AF displacement range. This indicates that this design can be scaled down and miniaturized when designing smartphone camera modules or compact biomedical cameras, and scaled up for larger and heavier lenses of CCTV and vehicle cameras. To miniaturize the MSM actuator system for smartphone applications, its height b_m should be reduced by choosing shorter MSM elements. This means that larger strain of MSM elements is required for sufficient AF displacement. However, low-weight lenses used in smartphones allow low-load operating curves in Fig. 6 to be chosen reducing the required magnetic field. Furthermore, the total reluctance of the magnetic circuit should be reduced by decreasing d_a and a_m. This leads to lower current required in smartphone MSM camera modules. Whereas this paper focuses on the mechanism that combines AF and OIS functions and its experimental verification, future work will elaborate on the exact design of smartphone MSM actuator system following the guidelines in Section IV of this paper.

C. CORRELATIONS BETWEEN MSM ALLOY PROPERTIES AND MSM ACTUATOR SYSTEM PERFORMANCE

This study identified a strong correlation between MSM alloy properties and the performance of the MSM actuator. First, MSM alloys with high available strain ε_{max} are desirable because the required height of the MSM actuator decreases as ε_{max} increases. Second, large magnetic stresses σ_{mag} are also desirable owing to their relationship with the output forces. Third, the twinning stress σ_{tw} increases the holding force but also increases the minimum current required to initiate the MSM element elongation, as illustrated by non-zero currents required for AF (Fig. 13) and OIS (Fig. 15) functions even at zero load. Hence, σ_{tw} should be carefully selected depending on the desired performance of the actuator system, specifically when large holding forces could be exploited.

The problem of the initial offset in the input current caused by the twinning stress has been studied previously and the use of a weak PM for generating a sufficient constant magnetic field has been proposed [28], [40]. However, this approach may result in non-zero stray magnetic fields produced by the actuator system. On the other hand, Type II MSM alloys that operate in significantly weaker magnetic fields could also provide a potential solution [41]. However, Type II alloys are still a subject of ongoing research, and Type II MSM actuators produce a negligible holding force owing to their low twinning stress. Nevertheless, this indicates that a breakthrough in material study research would also have a significant impact on the performance of MSM actuator technology.

The research area of MSM alloys is growing rapidly, and new alloys and promising alloy compositions are continuously being discovered [42], [43]. The desirable properties of MSM alloys for camera module applications reported in this paper provide important insights on the features of MSM alloys suitable for such applications, thereby presenting an

opportunity for high-impact collaborative research between electrical engineering and material study research societies.

VII. CONCLUSION

This paper presented a novel MSM actuator system for realizing a combined AF and OIS camera module. The proposed design only comprises two MSM actuators to realize both functions, thereby substantially reducing the number of required components and the complexity of the actuator system. Furthermore, the smart properties and holding forces associated with MSM elements provide an opportunity for a significant reduction in the energy consumption of the system.

The operating principles of the proposed MSM actuator system are discussed and verified using the data obtained from a verification prototype. Controlling the lengths of the MSM elements enables the realization of the AF function, whereas controlling the difference in their lengths results in lens barrel tilting, which translates into the OIS function. The relation between camera module performance and MSM element properties is also discussed, indicating a strong dependence of the size, lens weight, energy consumption, and output linearity of the camera module on the properties of the MSM alloy.

The results of this study indicate that the comparatively large forces produced by MSM elements enable the proposed actuator system to be scaled down for use in smartphone camera modules and mobile medical cameras, and to be scaled up to control the heavy lenses in larger stationary cameras such as CCTV. This indicates the significant potential applicability of MSM camera modules that combine multiple functions in a single actuator system.

REFERENCES

[1] H. Kim, J. Lee, S.-M. Hwang, and S. Cha, "Embedded camera module for automotive camera system," in *Proc. Pan Pacific Microelectron. Symp. (Pan Pacific)*, Big Island, HI, USA, Jan. 2016, pp. 1–7, doi: 10.1109/PanPacific.2016.7428414.

[2] I. Rivas-Blanco, C. López-Casado, C. J. Pérez-del-Pulgar, F. García-Vacas, J. C. Fraile, and V. F. Muñoz, "Smart cable-driven camera robotic assistant," *IEEE Trans. Human-Machine Syst.*, vol. 48, no. 2, pp. 183–196, Apr. 2018, doi: 10.1109/THMS.2017.2767286.

[3] C.-L. Hsieh, Y.-H. Chang, Y.-T. Chen, and C.-S. Liu, "Design of VCM actuator with L-shape coil for smartphone cameras," *Microsyst. Technol.*, vol. 24, no. 2, pp. 1033–1040, Feb. 2018, doi: 10.1007/s00542-017-3454-1.

[4] H.-S. Wang, K.-F. Qiu, and P. C.-P. Chao, "Five-axis stabilization system for a 2-DOF translational OIS," in *Proc. ICASI*, May 2017, pp. 1946–1949, doi: 10.1109/ICASI.2017.7988477.

[5] H. Gao, F. Zhang, E. Wang, B. Liu, W. Zeng, and Z. Wang, "Optimization and simulation of a voice coil motor for fuel injectors of two-stroke aviation piston engine," *Adv. Mech. Eng.*, vol. 11, no. 4, pp. 1–17, 2019, doi: 10.1177/1687814019846261.

[6] A. Sozinov, A. A. Likhachev, N. Lanska, O. Söderberg, K. Ullakko, and V. K. Lindroos, "Stress- and magnetic-field-induced variant rearrangement in Ni–Mn–Ga single crystals with seven-layered martensitic structure," *Mater. Sci. Eng., A*, vol. 378, nos. 1–2, pp. 399–402, Jul. 2004, doi: 10.1016/j.msea.2003.10.365.

[7] K. Majewska, A. Zak, and W. Ostachowicz, "Magnetic shape memory (MSM) actuators in practical use," *J. Phys., Conf. Ser.*, vol. 181, Aug. 2009, Art. no. 012073, doi: 10.1088/1742-6596/181/1/012073.

[8] A. Kazi, M. Honold, W. Rimkus, T. Lokner, M. Baeuml, and M. Koepfer, "SMA actuator for optical image stabilization," in *Proc. Actuator*, Bremen, Germany, 2018, pp. 25–27.

[9] S. J. Park and C. H. Park, "Suit-type wearable robot powered by shape-memory-alloy-based fabric muscle," *Sci. Rep.*, vol. 9, no. 1, pp. 1–8, Dec. 2019, doi: 10.1038/s41598-019-45722-x.

[10] S. Nemat-Nasser and W.-G. Guo, "Superelastic and cyclic response of NiTi SMA at various strain rates and temperatures," *Mech. Mater.*, vol. 38, nos. 5–6, pp. 463–474, May 2006, doi: 10.1016/j.mechmat.2005.07.004.

[11] T. Schiepp, M. Maier, E. Pagounis, A. Schluter, and M. Laufenberg, "FEM-simulation of magnetic shape memory actuators," *IEEE Trans. Magn.*, vol. 50, no. 2, pp. 989–992, Feb. 2014, doi: 10.1109/tmag.2013.2279205.

[12] H. Sayyaadi and H. Naderi, "Energy harvesting from plate using magnetic shape memory alloys," in *Proc. IcRoM*, 2019, pp. 229–235, doi: 10.1109/ICRoM.2018.8657576.

[13] F. Ehle, U. Neumeister, U. Keitel, and H. Neubert, "Self-sensing actuators based on ferromagentic shape memory alloys," in *Proc. Actuator*, Bremen, Germany, 2018, pp. 212–215.

[14] A. Hobza, C. L. Patrick, K. Ullakko, N. Rafla, P. Lindquist, and P. Müllner, "Sensing strain with Ni–Mn–Ga," *Sens. Actuators A, Phys.*, vol. 269, pp. 137–144, Jan. 2018, doi: 10.1016/j.sna.2017.11.002.

[15] C.-L. Hsieh, H.-Y. Wang, Y.-H. Chang, and C.-S. Liu, "Design of VCM actuator with the chamfered edge magnet for cellphone," *Microsyst. Technol.*, vol. 23, no. 12, pp. 5293–5302, Dec. 2017, doi: 10.1007/s00542-017-3307-y.

[16] B. Holz, H. Janocha, and L. Riccardi, "Compact MSM actuators—Concept for highest force exploitation," in *Proc. Actuator*, Bremen, Germany, 2012, pp. 1–4.

[17] N. Gabdullin and S. H. Khan, "Electromagnetic and thermal analyses of high-performance magnetic shape memory actuators for valve applications," *IEEE Trans. Magn.*, vol. 52, no. 9, pp. 1–6, Sep. 2016, doi: 10.1109/TMAG.2016.2563406.

[18] E. Pagounis, R. Chulist, M. J. Szczerba, and M. Laufenberg, "High-temperature magnetic shape memory actuation in a Ni–Mn–Ga single crystal," *Scripta Mater.*, vol. 83, pp. 29–32, Jul. 2014, doi: 10.1016/j.scriptamat.2014.04.001.

[19] S. J. Murray, M. Marioni, S. M. Allen, R. C. O'Handley, and T. A. Lograsso, "6% magnetic-field-induced strain by twin-boundary motion in ferromagnetic Ni–Mn–Ga," *Appl. Phys. Lett.*, vol. 77, no. 6, pp. 886–888, Aug. 2000, doi: 10.1063/1.1306635.

[20] A. Sozinov, N. Lanska, A. Soroka, and W. Zou, "12% magnetic field-induced strain in Ni–Mn–Ga-based non-modulated martensite," *Appl. Phys. Lett.*, vol. 102, no. 2, Jan. 2013, Art. no. 021902, doi: 10.1063/1.4775677.

[21] K. Ullakko, L. Wendell, A. Smith, P. Müllner, and G. Hampikian, "A magnetic shape memory micropump: Contact-free, and compatible with PCR and human DNA profiling," *Smart Mater. Struct.*, vol. 21, no. 11, Nov. 2012, Art. no. 115020, doi: 10.1088/0964-1726/21/11/115020.

[22] Z. Li, Y. Zhang, C. Esling, X. Zhao, and L. Zuo, "Twin relationships of 5M modulated martensite in Ni–Mn–Ga alloy," *Acta Mater.*, vol. 59, no. 9, pp. 3390–3397, May 2011, doi: 10.1016/j.actamat.2011.02.014.

[23] O. Heczko, L. Straka, and H. Seiner, "Different microstructures of mobile twin boundaries in 10M modulated Ni–Mn–Ga martensite," *Acta Mater.*, vol. 61, no. 2, pp. 622–631, Jan. 2013, doi: 10.1016/j.actamat.2012.10.007.

[24] L. Straka, H. Hänninen, A. Soroka, and A. Sozinov, "Ni–Mn–Ga single crystals with very low twinning stress," *J. Phys., Conf. Ser.*, vol. 303, Jul. 2011, Art. no. 012079, doi: 10.1088/1742-6596/303/1/012079.

[25] M. Chmielus, C. Witherspoon, R. C. Wimpory, A. Paulke, A. Hilger, X. Zhang, D. C. Dunand, and P. Müllner, "Magnetic-field-induced recovery strain in polycrystalline Ni–Mn–Ga foam," *J. Appl. Phys.*, vol. 108, no. 12, Dec. 2010, Art. no. 123526, doi: 10.1063/1.3524503.

[26] D. E. Soto-Parra, E. Vives, D. González-Alonso, L. Mañosa, A. Planes, R. Romero, J. A. Matutes-Aquino, R. A. Ochoa-Gamboa, and H. Flores-Zúñiga, "Stress- and magnetic field-induced entropy changes in Fe-doped Ni–Mn–Ga shape-memory alloys," *Appl. Phys. Lett.*, vol. 96, no. 7, Feb. 2010, Art. no. 071912, doi: 10.1063/1.3309755.

[27] V. A. Chernenko, M. Chmielus, and P. Müllner, "Large magnetic-field-induced strains in Ni–Mn–Ga nonmodulated martensite," *Appl. Phys. Lett.*, vol. 95, no. 10, Sep. 2009, Art. no. 104103, doi: 10.1063/1.3227661.

[28] B. Holz, L. Riccardi, H. Janocha, and D. Naso, "MSM actuators: Design rules and control strategies," *Adv. Eng. Mater.*, vol. 14, no. 8, pp. 668–681, Aug. 2012, doi: 10.1002/adem.201200045.

[29] A. Tüysüz, S. Breisch, and T. Molter, "Linear actuator utilizing magnetic shape memory material," in *Proc. LDIA*, Neuchatel, Switzerland, 2019, pp. 1–4, doi: 10.1109/ldia.2019.8771026.
[30] L. K. Lai and T. S. Liu, "Design of auto-focusing modules in cell phone cameras," *Int. J. Smart Sens. Intell. Syst.*, vol. 4, no. 4, pp. 568–582, 2011, doi: 10.21307/ijssis-2017-457.
[31] C. S. Liu and P. D. Lin, "High positioning repeatability of miniature actuator," *Sensors Mater.*, vol. 20, no. 7, pp. 319–326, 2008, doi: 10.18494/sam.2009.563.
[32] N. Gabdullin, "Modelling and design of high-speed, long-lifetime and large-force electromagnetic actuators based on magnetic shape memory alloys," M.S. thesis, Univ. London, Gurugram, Haryana, 2016, pp. 1–184. [Online]. Available: https://openaccess.city.ac.uk/id/eprint/16130/
[33] G. Slemon, *Electric Machines and Drives*, 1st ed. New York, NY, USA: Addison-Wesley Publishing Company, 1992.
[34] L. Righi, F. Albertini, E. Villa, A. Paoluzi, G. Calestani, V. Chernenko, S. Besseghini, C. Ritter, and F. Passaretti, "Crystal structure of 7M modulated Ni–Mn–Ga martensitic phase," *Acta Mater.*, vol. 56, no. 16, pp. 4529–4535, Sep. 2008, doi: 10.1016/j.actamat.2008.05.010.
[35] N. Gabdullin and S. H. Khan, "Study of non-homogeneity of magnetic field distribution in single-crystal Ni–Mn–Ga magnetic shape memory element in actuators due to its anisotropic twinned microstructure," *IEEE Trans. Magn.*, vol. 53, no. 3, Mar. 2017, Art. no. 4900108, doi: 10.1109/TMAG.2016.2640201.
[36] N. Gabdullin and S. H. Khan, "Study of magnetic field distribution in anisotropic single twin-boundary magnetic shape memory (MSM) element in actuators," *J. Phys., Conf. Ser.*, vol. 903, Oct. 2017, Art. no. 012012, doi: 10.1088/1742-6596/903/1/012012.
[37] L. Riccardi, T. Schiepp, B. Holz, M. Maier, H. Janocha, and M. Laufenberg, "A modular, energy efficient actuator based on magnetic shape memory alloys," in *Proc. Actuator*, Bremen, Germany, 2014, pp. 112–115.
[38] A. A. T. M. Delissen, G. Radaelli, and J. L. Herder, "Design and optimization of a general planar zero free length spring," *Mechanism Mach. Theory*, vol. 117, pp. 56–77, Nov. 2017, doi: 10.1016/j.mechmachtheory.2017.07.002.
[39] G. Keung and C. Chen, "Novel design of an adjustable constant force mechanism based on cam and spring," in *Proc. IFToMM World Congr. Mechanism Mach. Sci.*, in Mechanisms and Machine Science, vol. 73, 2019, pp. 1481–1490, doi: 10.1007/978-3-030-20131-9_146.
[40] M. Raab and W. Schinkoethe, "Active gravity compensation actuator using the multistability of magnetic shape memory," in *Proc. Actuator*, Bremen, Germany, 2018, pp. 39–42.
[41] D. Kellis, A. Smith, K. Ullakko, and P. Müllner, "Oriented single crystals of Ni–Mn–Ga with very low switching field," *J. Cryst. Growth*, vol. 359, pp. 64–68, Nov. 2012, doi: 10.1016/j.jcrysgro.2012.08.014.
[42] S. Rößler, C. Koz, Z. Wang, Y. Skourski, M. Doerr, D. Kasinathan, H. Rosner, M. Schmidt, U. Schwarz, Ulrich K. Rößler, and S. Wirth, "Two types of magnetic shape-memory effects from twinned microstructure and magneto-structural coupling in $Fe_{1+y}Te$," *Proc. Nat. Acad. Sci. USA*, vol. 116, no. 34, pp. 16697–16702, 2019, doi: 10.1073/pnas.1905271116.
[43] F. Nilsén, J. Lehtonen, Y. Ge, I. Aaltio, and S.-P. Hannula, "Highly porous spark plasma sintered Ni–Mn–Ga structures," *Scripta Mater.*, vol. 139, pp. 148–151, Oct. 2017, doi: 10.1016/j.scriptamat.2017.06.040.

NIKITA GABDULLIN (Member, IEEE) received the B.S. and M.S. degrees in electrical engineering from National Research University (MPEI), Moscow, Russia, in 2010 and 2012, respectively, and the Ph.D. degree in electrical and electronic engineering from the City, University of London, London, U.K., in 2017. He is currently a Postdoctoral Researcher with Chung-Ang University, Seoul, South Korea. His research interests include analytical and numerical modeling of electromagnetic fields, novel electrical machine design, multi-physics and coupled problem analysis, application of piezoelectric, magnetic shape memory, and other smart materials in energy-efficient electromagnetic devices.

HAMZA AHMAD (Graduate Student Member, IEEE) received the B.S. degree in electrical engineering from the Pakistan Institute of Engineering and Applied Sciences (PIEAS), Pakistan, in 2018. He is currently pursuing the M.S. degree with Chung-Ang University, Seoul, South Korea. He is also a Graduate Research Assistant with Chung-Ang University. His research interests include design and optimization of electrical machines and applications of electromagnetic smart materials.

JONGSUK RO (Member, IEEE) received the B.S. degree in mechanical engineering from Han-Yang University, Seoul, South Korea, in 2001, and the Ph.D. degree in electrical engineering from Seoul National University (SNU), Seoul, in 2008. From 2008 to 2012, he was a Senior Engineer with the Research and Development Center, Samsung Electronics. From 2012 to 2013, he was a Postdoctoral Fellow with the Brain Korea 21 Information Technology, SNU. From 2013 to 2016, he worked as a BK Assistant Professor with the Brain Korea 21 Plus, SNU. He was a Researcher with the Electrical Energy Conversion System Research Division, Korea Electrical Engineering and Science Research Institute, in 2013. He was with the University of Bath, Bath, U.K., in 2014. He is currently an Associate Professor with the School of Electrical and Electronics Engineering, Chung-Ang University, Seoul.